Unveiling the topological structure of chaotic flows from data

Denisse Sciamarella and G. B. Mindlin
Departamento de Física, Facultad de Ciencias Exactas y Naturales, Universidad de Buenos Aires, Pab I, Ciudad Universitaria, Casilla de Correo 1428, Buenos Aires, Argentina
(Received 13 December 2000; published 21 August 2001)

We report the analysis of branched manifolds through homologies, in order to extend the range of applicability of the topological approach to the analysis of chaotic data. Analytic and numerical cases are discussed.

DOI: 10.1103/PhysRevE.64.036209 PACS number(s): 05.45.Pq, 47.52.+j, 02.40.Sf

I. INTRODUCTION

Some of the results obtained by dynamicists in the past 20 years have had a profound impact in the natural sciences, particularly, the idea that simple deterministic rules could give rise to complex, long-term unpredictable behavior (chaos) [1]. Since then, we have been faced with two main challenges when dealing with chaotic data: how to unveil the simple deterministic rule mentioned above, and how to validate it from the data.

One of the most popular approaches to analyzing chaotic data is of a metric nature. The stretching and squeezing in phase space associated with the mechanism responsible for the hypersensitivity to initial conditions give rise to fractal properties of the invariant set to which the observed trajectory belongs. A quantity describing this fractality (e.g., fractal dimension) can be an important way to estimate the number of relevant variables affecting the deterministic rule, the degree of complexity, etc. Yet it does not enlighten the geometric nature of the rule [1].

In recent years, another complementary way to analyze data was proposed, aimed at describing the topological structure of the flow. For three-dimensional systems, the way in which the periodic orbits are knotted and linked among themselves can be used in order to classify dynamic systems [2,3], and successful implementations of this method were obtained for real data (i.e., experimental data) [1]. Yet the applicability of this method is restricted both by the dimensionality (three) and the possibility of reconstructing good approximations of the unstable periodic orbits coexisting with the strange attractor (long time series data and reasonably free of noise). In order to overcome these difficulties, it was proposed to analyze the structure of the invariant manifold on which the data lie by means of other topological invariants, namely its set of homology groups. Periodic and quasiperiodic solutions were studied in this way [5].

We build on the previous efforts mentioned above, implementing a way to decompose the invariant manifold associated to a chaotic solution under study in building blocks. These building blocks constitute complexes, and algorithmically we handle the gluing prescriptions followed to assemble them. The description of the complex (which turns out to be a rough skeleton of the manifold visited by the chaotic trajectory) is performed by means of homologies, chain groups, and explicit boundary maps.

We report the study of two chaotic solutions (one of them the result of integrating numerically a three-dimensional set of ordinary differential equations, the second one from a four-dimensional system). A study of experimental data from the human voice (pressure fluctuations as a voiced sound is pronounced) has been reported in [4].

This paper is organized as follows. In Sec. II, we provide a summary of the mathematical background needed to follow this work. In Sec. III, we review the role of templates in analyzing chaotic data and describe some of these branched manifolds in terms of homologies. Section IV contains a description of the way in which we perform our cell decomposition. In Secs. V and VI, we report the study of two chaotic solutions (one of them the result of integrating numerically a three-dimensional ordinary differential equation, the second one from a four-dimensional system). We close our work with Sec. VII, in which we report our conclusions.

II. HOMOLOGIES

To determine whether two given spaces are topologically equivalent is a difficult problem. The combinatorial approach to topology consists in describing how to glue a set of building blocks in order to construct an object equivalent to the one under study [6].

The building blocks that we mentioned above are the *n*-cells, which are sets that (a) can be mapped (through a continuous invertible map) into the interior of an *n*-disk, and (b) have their boundaries or frontiers divided into finite numbers of lower-dimensional cells, called faces. A point then is a 0-cell, a line segment joining two points is a 1-cell, etc. Cells can be assembled into a complex, which is a finite set of cells such that (a) the faces of the cells are elements of the complexes and (b) the interiors of two cells in a complex do not intersect. The dimension of a complex is the dimension of its highest-dimensional cell. A two-dimensional complex is said to be oriented if each 1-cell is given a direction (the edge point of which is terminal) as well as each 2-cell (clockwise or anticlockwise).

A directed complex allows us to define integral chains, which are sums $C=a_1\sigma_1+\cdots+a_n\sigma_n$, with σ_i and a_i $(i=1,\ldots,n)$, *k*-cells, and integers, respectively. We can define a sum of *k*-cells in a directed complex by adding the coefficients, and therefore the *k*-chains in a complex can be dressed with a group structure. In other words, given a di-

rected complex K, $C_k(K)$ denotes the groups of all the k-chains for $k=0,1,\ldots,\dim(K)$. This group constitutes our first step toward building algebraic structures that will allow us to characterize the set under study.

So far we have dealt with building blocks (cells). But in order to assemble the complex, we have to describe how to glue the blocks (for example, which point face of a 1-cell has to be attached to a given cell, or which 1-cell is shared by two given 2-cells). The first step toward this description is then to be able to pick the faces of a given cell. This can be achieved by what is called a boundary map, ∂, which returns, when applied to a given cell, the chain of all the $(k-1)$-cells that are its faces. One can extend the action of the map to k-chains trivially. We denote by $\partial: C_k(K) \rightarrow C_{k-1}(K)$ the map in which

$$\partial(C=a_1\sigma_1+\cdots+a_n\sigma_n)=a_1\partial(\sigma_1)+\cdots+a_n\partial(\sigma_n). \tag{1}$$

This map will allow us to pick up specific k-chains, namely, the ones such that $\partial(C)=0$. These are called k-cycles and are denoted by Z_k. Among the k-cycles, we can distinguish the ones that are borders of a higher-dimensional cell, and we call the set of all these cycles the boundary group B_k. Notice that these algebraic tools will allow us to identify the ''holes'' in our set (a hole is a cycle that is not the border of a higher-dimensional cell). Finally, we call two k-chains homologous if $C_1-C_2=\partial(D)$ for some $(k+1)$-chain D. The group of equivalence of elements of Z_k with the homology relation is called the homology group $H_k(K)$. The main motivation for introducing this equivalence relation is to build an algebraic structure that does not depend on the complex used to model the object under study.

A convenient way of denoting cells in a complex is to provide a list of the vertices of each cell. The ordering of the vertices produces a natural orientation, which contributes to the description of a directed complex. Let us denote by $\langle v_0\rangle$ the vertex or 0-cell v_0; $\langle v_0,v_1\rangle$ would be the edge of a 1-cell running from v_0 to v_1, and so on. There are often advantages (usually theoretical and not practical) in using simplex complexes, i.e., complexes built up with k-cells (called k-simplex) that have exactly $k+1$ vertices. Thus, if the complex is simplex, the number of vertices of a simplex tells one immediately the dimension of the cell. This greatly simplifies, for instance, the computation of the homology groups H_k.

From the definition of the homology groups, it is clear that the construction of these layered invariants $[H_k(K)]$ can be obtained algorithmically once the boundary maps of a given complex are provided, whether the complex is simplex or not (in fact, throughout the rest of this paper we will not assume that our cells are simplex. The additional complexity of an algorithm handling nonsimplex cells pays off when one attempts to describe through homologies an invariant set, as we will see in Sec. IV). The algebraic manipulation of the list of oriented vertices that composes each cell in the complex allows us, through environments such as MATHEMATICA, to build all the homology groups quite easily. The basic steps to compute them are as follows:

(i) Reading the list of vertices of every cell to construct a matrix representation of the boundary maps, taking into account that the cells need not be simplex; (ii) computing the B_k groups as the (lattice) linearly independent rows of these boundary map matrices; (iii) calculating the Z_k groups as the null spaces of the transpose of the boundary map matrices; (iv) expressing the elements of B_k (the k-borders) in terms of the elements of Z_k (the k-cycles), so as to find which k-cycles are homologous to others; (v) appending in H_k those k-cycles that are homologically independent; (vi) if the cells of the complex have all the same orientation (as will result from the algorithm in Sec. IV), the torsion properties of the complex are calculated by the recognition of integer multiples of chains within the chain summing up all the k-borders of the complex. Let us call these chains the orientability chains.

Notice that step (vi) renders the description of the topological properties of the manifold more complete, since homology groups do not tell, for instance, a cylinder from a Moebius strip, while the identification of the orientability chains does provide this distinction. In the Appendix, an example is spelled out. In the following section, we will compute explicitly the chain, boundary, cyclic, and homology groups for several simple complexes, which are of major interest in dynamics. These examples will enable us to become familiar with the definitions stated above, as well as with the calculations that we will be reporting throughout this work.

III. BRANCHED MANIFOLDS AND TEMPLATES

In the early 1980s, Birman and Williams introduced the idea of knot holders, which are branched manifolds able to hold all the periodic orbits coexisting in a hyperbolic invariant set [7]. They introduced this structure as the result of an equivalence relation between points in the invariant set defined as follows: two points are equivalent if they belong to the stable manifold of some point in the invariant set. This collapse would not affect periodic orbits (two periodic orbits obviously do not have the same future). Even if the definition of these objects is performed in the context of hyperbolic sets, many highly dissipative flows containing strange attractors display a ''mask'' structure that closely resemble a knot holder.

In the 1990s, it was proposed that building knot holders compatible with the unstable periodic orbits coexisting with a strange attractor could help us to understand the geometric mechanisms responsible for the observed behavior [2,3]. In what follows, we will describe some branched manifolds in terms of the layered invariants introduced in the preceding section.

Let us begin with the three manifolds displayed in Fig. 1. All of them are compatible with a stretching and folding such as are present in the suspension of a horseshoe map [8]. In the first example, the cell denoted by τ is attached through the one-dimensional cell a to the cell σ with a gluing direc-

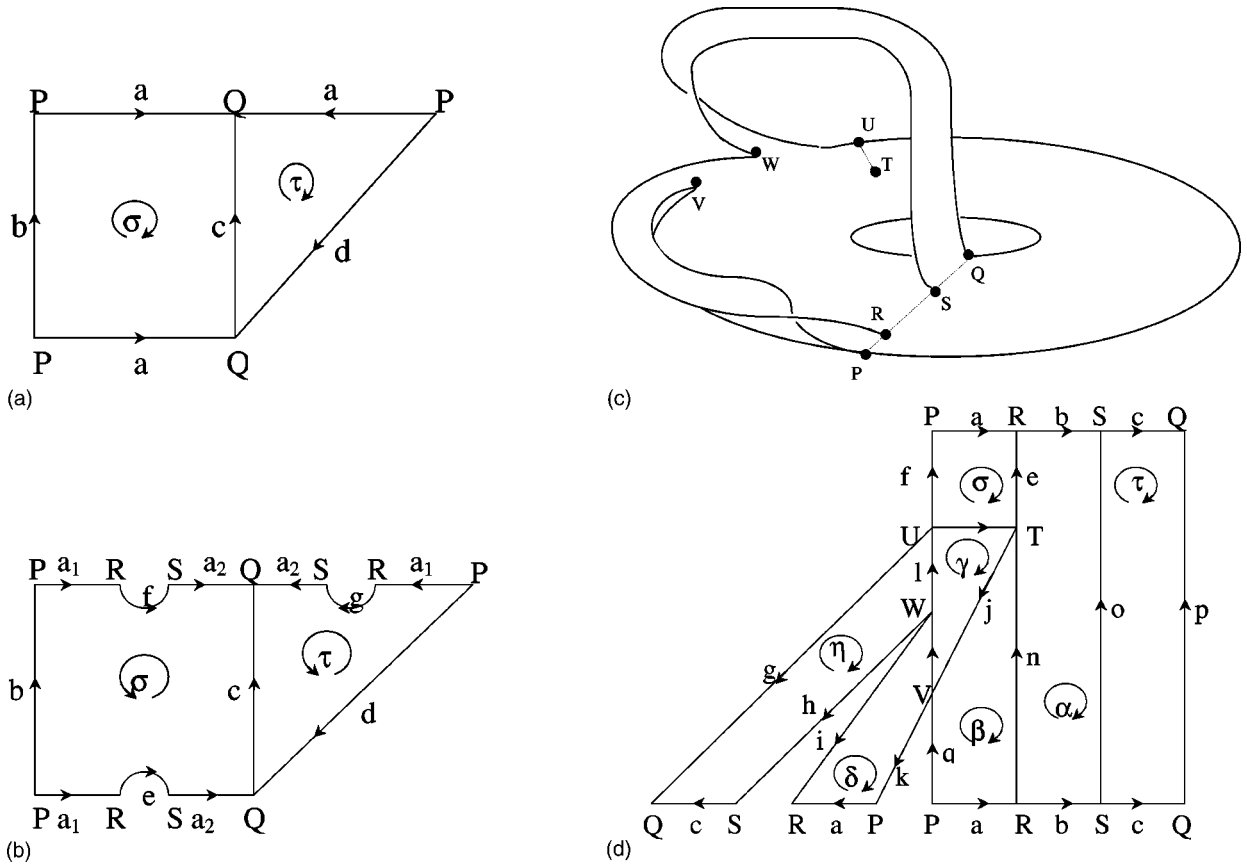

FIG. 1. A simple branched manifold, compatible with a Smale stretching and folding (a). In this branched manifold, two small disks were removed at a point in *a*. This elimination demonstrates the branched nature of the set, as just one disk is not enough to deplete the chosen point from neighbors (b). (c) A branched manifold with two handles and (d) its cell decomposition.

tion that enlightens the folding taking place. In order to compute the *k*-homology groups of this branched manifold, we proceed as follows. First, we compute the C_k groups. The 0-cells are P and Q, the 1-cells are a, b, c, and d, while the 2-cells are τ and σ. The action of the boundary maps on these cells is the following. Trivially, $\partial(P)=\partial(Q)=0$. As the upper and lower 1-cells are identified (in a), we see that $\partial(b)=\partial(c)=0$. The action of the boundary map on a is $\partial(a)=Q-P=\partial(d)$, and therefore $\partial(a-d)=0$. The boundary map acting on the two cells gives $\partial(\sigma)=-a+b+a-c=b-c$ (hence $b\approx c$), and $\partial(\tau)=a+c-d$ (hence $c\approx d-a$).

We can summarize these results in the following way:

$$C_0=[[P,Q]],C_1=[[a,b,c,d]],C_2=[[\tau,\sigma]],$$

$$Z_0=[[P,Q]],Z_1=[[b,c,a-d]],Z_2=0,$$

$$B_0=[[Q-P]],B_1=[[b-c,a+c-d]],B_2=0.$$

We now take the Z_k groups modulo the equivalences dictated by the B_k, which gives rise to

$$H_0=[[P,Q:P\sim Q]]\approx\mathcal{Z}^1,H_1=[[b,c,a-d:c\sim b,a-d\sim b]]\approx\mathcal{Z}^1,H_2=0,$$

with $\mathcal{Z}$ the groups of integers. Therefore, this layered group structure indicates that the branched manifold has a single connected component, that one homologically independent loop exists that does not border any 2-cell, and that the complex encloses no cavities.

The branched manifold displayed in Fig. 1(b) is similar to the one described above but two small disks have been removed in the neighborhood of a point in *a*. The elimination of these points enlightens the branched nature of the set, as just one disk is not enough to deplete the chosen point from neighbors. The final homology groups are

$$H_0=[[P]]\approx\mathcal{Z}^1,H_1=[[b,c,f-g]]\approx\mathcal{Z}^3,H_2=0.$$

Notice that while the first manifold was homologic to the cylinder, this one is not due to the additional single loops, which show the branched nature of the set.

Our final example is displayed in Figs. 1(c) and 1(d). Both figures represent the same object, although the one in one dimension (1D) contains an explicit cell decomposition that we used to compute its homology. Proceeding as in the first example, we obtain the following group structure:

$$H_0=[[A]]\approx\mathcal{Z}^1, H_1=[[e+n, a-e+j+k, -b-c-d-e+g]]\approx\mathcal{Z}^3, H_2=0.$$

The meaning of the three loops implied by the H_1 homology group can be visualized from Fig. 1(c). The first loop is placed within the disk, the second one that visits the handle glued to the external part of the disc, while the last loop exists in the second handle.

Branched manifolds have been used in the past to identify the geometric mechanisms responsible for the complexity of flows. The idea was to identify in a flow the unstable orbits closely visited by a trajectory, and to check whether those orbits could be placed in a given branched manifold, i.e., whether they were compatible. In this spirit, our aim is to study the compatibility of invariant manifolds obtained numerically with simple models. Let us remark that the examples shown above are locally two-dimensional. Yet these tools will allow us to go beyond the situations that could be addressed by analyzing the organization of periodic orbits. For example, a Klein bottle is a locally two-dimensional set that cannot be embedded in three dimensions.

IV. CELL DECOMPOSITION

As mentioned in Sec. II, our approach to describing an invariant set consists in decomposing it in building blocks, keeping track of the gluing prescriptions that are necessary to assemble it. Those building blocks are cells, that is, sets that are homeomorphic to the interiors of n-disks. Basically then, one needs to select a sufficiently large number of points that can be used as the centers of disks enclosing their neighbors so that every point in the invariant set under study is within at least one cell.

We will describe our procedure, which closely follows [5]. We take a first point, and sort the rest of the points according to their distance from the first one. A criterion is chosen to define the largest radius such that the points enclosed in the set are good approximations to a d-dimensional Euclidean set (the dimension of the cells d being lower than or equal to the dimension of phase space n). All the points are labeled with an index that indicates their pertinence to the cell based on the initial point. Successive centers are taken so that they are least separated from the previously chosen center, until every point in the invariant set under study is in at least one cell. In this way, we assign a set of integers to each point of the set under study, which indicates the set of cells to which it belongs.

Let us describe the criterion used to define the largest number of points considered so that the points enclosed in the set are good approximations to a d-dimensional Euclidean set. Provided that the density of points around a given center (x_0) is approximately uniform, we choose a reasonable limit for the maximum $(N_{\max})$ and minimum $(N_{\min})$ number of points to be included in a cell. Next, we consider the set of points $\{x_i, i=N_{\min}, \ldots, N_{\max}\}$, where i labels the points in the file under analysis, in order of increasing distance from x_0 (the center). In order to check for which value of i the set x_i best approximates a d-dimensional Euclidean set, we inspect the distribution of the points in the set x_i. If the set of points in R^n is a good approximation to a d-dimensional Euclidean set, then the square roots of d of the second moments of the points in a small ball of radius R decrease linearly as $R\to 0$, while $n-d$ decrease to zero as higher powers of R. In order to inspect for which value of N in $\{x_i, i=0\cdots N\}$ this property is best fulfilled, we inspect the singular values of the matrix:

$$X_{i,j}=(x_{i,j}-x_{0,j}) \tag{2}$$

with $i=1,2,\ldots,N$ (N is the number of points under inspection) and $j=1,2,\ldots,n$ (with n the phase-space dimension). Here, the $(x_{0,1}, x_{0,2}, \ldots, x_{0,n})$ are the coordinates of the centers of our cells, and the $(x_{i,1}, x_{i,2}, \ldots, x_{i,n})$ denote the coordinates of the other N points in the file under analysis, in order of increasing distance from the center. For different values of N, we obtain different sets of singular values. Thus we define a d-dimensional cell as the set of points $\{x_i, i=0\cdots N_c\}$ for which the d largest singular values of X present the best linear regression coefficients $(N_{\min}\leqslant N_c\leqslant N_{\max})$. Note that less general criteria may also prove to be effective: for the examples considered in [4], the size of a cell could be determined by direct comparison of the singular values (points around a center were grouped in a cell when the third largest singular value was smaller than a given fraction of the second largest one).

Once an appropriate cell decomposition is attained, the next step is the construction of the complex of assembled cells. In Ref. [5], an $(n-1)$-cell was recognized whenever there was at least one point belonging to the intersection of n cells. This method has the advantage that the cells that are obtained are simplices (i.e., cells with a minimal number of faces), which greatly simplifies the calculation of the boundary maps. But we found that this method had several shortcomings: branches of the invariant set that could be locally approximated by planes would give rise to filamentations (two consecutive 2-cells would be associated to a 1-cell). Another problem of this method is that it disregards points belonging to intersections of a number of cells exceeding the dimension of the phase space, creating holes and overlaps that change the homology of the set under study. These imperfections in the construction of the complex are serious because they lead to a representation that will not present the same topological properties of the invariant set under study. In other words, the complex we attempt to construct is merely a model of the structure of the strange attractor that we want to describe, and consequently the gluing prescriptions must preserve the topology of the original manifold.

In view of these facts, we preferred to explicitly build all the faces of a cell by calculating the convex hull for the points of the cell that provide the intersections with neighboring cells, at the expense of the simple algorithms valid for simplices. The convex hull of a set of points S is a list with fixed orientation of the vertices forming the boundary of the smallest set containing S. In other words, we respect the

nonsimplex nature of a given cell, if this is necessary to account for a given gluing prescription.

It is worth noting that in the case of a small data file, when a region of the attractor has a very low natural measure and thus is seldom visited, there is a chance that additional independent loops are created. If this is the case, the caricature of the attractor might depend on the data set and, consequently, all we can achieve is an identification of compatibility of the reconstructed branched manifold with one associated to a specific stretching and folding mechanism.

V. TOY MODEL I

In Sec. III, we reported the calculation of the homology groups for different branched manifolds. Now we want to proceed to compute these quantities from data. In this section, we will deal with an easy case: data coming from a numerical experiment, free of noise. Moreover, instead of studying a standard test bench for nonlinear dynamics (such as the Rossler equations or the Lorenz ones), we will work with the flow that is obtained after the integration of the following set of ordinary differential equations [9]:

$$
\begin{aligned}
x' &= -(z+2)d(x-a)+(2-z)\{\alpha(x-2)-\beta y-\alpha(x-2)\\
&\quad\times[(x-2)^2+y^2/R^2]\},\\
y' &= -(z+2)(y-b)+(2-z)\{\beta(x-2)-\alpha y-\alpha y[(x-2)^2\\
&\quad+y^2/R^2]\},\\
\epsilon z' &= (4-z^2)[z+2-m(x+2)]-\epsilon c z
\end{aligned}
\tag{3}
$$

with the parameter values listed in the caption of Fig. 2. This system was chosen for the following reason: its dynamics consists on a fast alternation between two dynamical regimes (one with $z\approx 2$ and another one with $z\approx -2$), as in a standard relaxation oscillation. In each of the two dimensional manifolds in which the system exists most of the time, the behavior can be easily prescribed [in this case, the system evolves to a stable fixed point at $(x_u, y_u, z_u) \approx (a, b, 2)$ in the upper branch , which can never be reached, while in the lower branch the flow is ruled by an unstable focus at $(x_l, y_l, z_l) \approx (2, 0, -2)$]. This is an example of a systematic way [8] to construct homoclinic attractors and chaotic flows: in our case, it helps us to build chaotic flows with desired topological properties. Notice that with properly chosen parameters, this system should present chaotic solutions of a Shilnikov-type, as it consists of a ''switch'' that reinjects the flow expelled by a (saddle) focus back to its neighborhood along its one-dimensional attracting manifold.

In Fig. 2(b), we display a set of 11 patches. Each is the result of joining the vertices that were selected as mentioned in Sec. IV. They constitute a rough caricature of the strange attractor displayed in Fig. 2(a), but reflect the way in which the covering cells are connected.

As mentioned in Sec. IV, we chose a criterion to define the largest radius so that the points enclosed in the set are good approximations to a d-cell. The dimension d is provided by the number of singular values that can be effectively approximated by a linear function in terms of the number of points forming the smallest admissible cell. For this toy model, $d=2$ while $n=3$ because the system treated is very dissipative, but nothing prevents the construction of complexes in the case of manifolds for which cells live in a Euclidean space of the same dimension of phase space. This criterion allows us to decompose the invariant set in 22 2-cells. Notice that in Fig. 2(b), only 11 are displayed for simplicity (they constitute a complex of the same homological type as the original one).

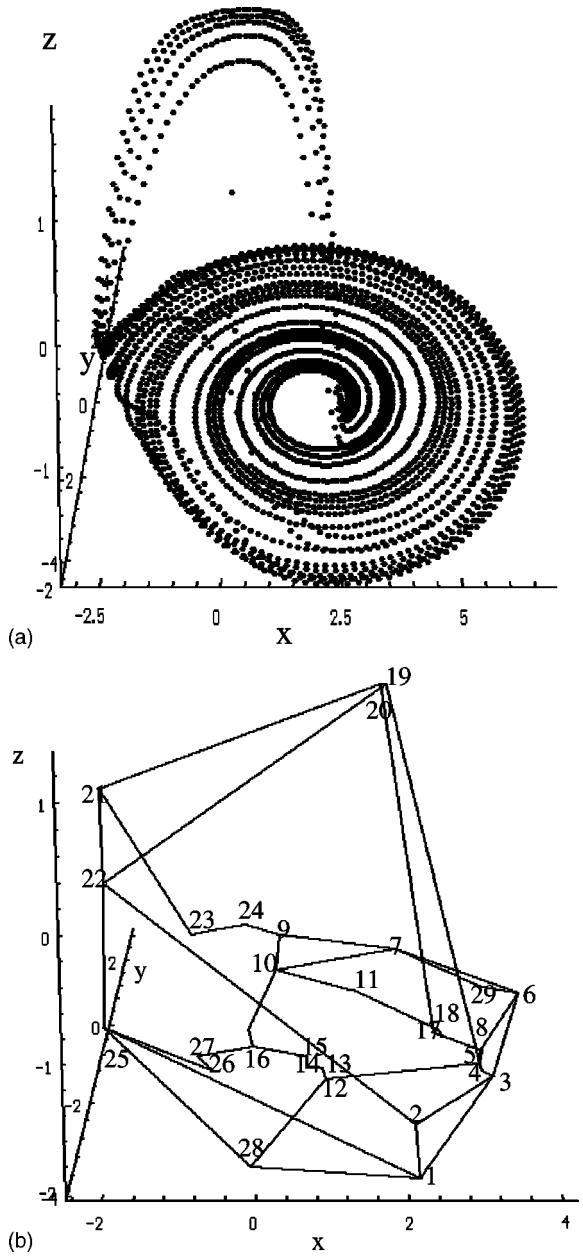

FIG. 2. The strange attractor generated by the integration of the system of Eq. (2), with the following set of parameters: $a=7$, $b=1.435$, $c=1$, $d=1.5$, $m=1.543$, $R=6$, $\alpha=0.5$, $\beta=4$, $\epsilon=0.15$ (a). Display of 11 cells obtained by joining the vertices that were selected in Sec. IV.

The vertices of the 2-cells displayed are arbitrarily labeled with numbers from 1 to 26, as shown in Table I. From

TABLE I. Vertices of the oriented cells corresponding to the cell decomposition of the strange attractor shown in Fig. 2(b).

Cell	Vertices
1	28,1,2,3,4,5,12
2	1,2,3
3	4,5,8,6,3
4	5,8,17,20,19
5	8,17,18,11,10,7,29,6
6	7,29,6
7	10,9,7
8	10,9,24,23,21,22,25,26,27,16
9	21,22,19,20
10	22,25,1,2
11	25,28,12,13,14,15,16,27,26

this table, one can compute the n-chain groups, the B_n groups, etc. But as we mentioned in Sec. II, a geometric description of the gluing of the n-cells, which is independent of the particular cell decomposition, can only be achieved through the calculation of the homologies. The content of Table I is enough to determine that the n-homology groups ($H_n's$) of this complex are

$$H_0 \approx \mathcal{Z}, H_1 \approx \mathcal{Z}^3, H_2 \approx 0,$$

where $\mathcal{Z}$ is generated by one of the vertices (for example, [26]), and the three loops of H_1 are generated by the following cycles, written as oriented 1-chains: the first loop is $L_1 = \langle 3,4\rangle - \langle 3,6\rangle + \langle 4,5\rangle + \langle 5,8\rangle - \langle 6,7\rangle - \langle 7,9\rangle + \langle 8,17\rangle - \langle 9,24\rangle + \langle 17,20\rangle + \langle 20,21\rangle + \langle 21,23\rangle + \langle 23,24\rangle$, the second one is $L_2 = -\langle 1,2\rangle + \langle 1,3\rangle - \langle 2,22\rangle + \langle 3,4\rangle + \langle 4,5\rangle + \langle 5,19\rangle + \langle 19,22\rangle$, and the third one is $L_3 = \langle 3,4\rangle - \langle 3,6\rangle + \langle 4,5\rangle + \langle 5,12\rangle - \langle 6,7\rangle - \langle 7,10\rangle - \langle 10,16\rangle + \langle 12,13\rangle + \langle 13,1\rangle + \langle 14,15\rangle + \langle 15,16\rangle$.

In summary, an analysis of the complex built from gluing the cells that locally cover the data indicates that the dynamics takes place close to a branched manifold constituted by only one connected piece, in which three nonequivalent (through homology) loops exist, and that it encloses no cavities. The explicit construction of the loops that generate H_1 allows us to unveil the structure of the branched manifold: it consists of a disk on which two strips are attached. This should be compared with our third theoretical example in Sec. III.

VI. TOY MODEL II

As mentioned in the Introduction, the topological approach to the study of chaotic time series data was based on the description of the organization of the periodic solutions visited by the trajectory under study. Knot theoretical tools were used to characterize this organization, which could eventually be summarized by the description of the templates that were able to hold the periodic solutions.

The price to be paid for the elegance that knot theory adds to the field is a strong restriction of the range of validity of the approach: a closed curve is no longer knotted in a space of dimension larger than 3. Even flows as simple as the ones that can take place on a Klein bottle cannot be studied with knot theoretical tools; a Klein bottle, which is a locally two-dimensional object, cannot be embedded in three dimensions (without self-intersections).

Our second example consists therefore of a chaotic flow that is built, as in the previous case, by dynamically connecting slow building blocks with simple dynamics. The dynamic system under study is

$$\begin{aligned} x' &= -(z+2)d\{x-[a+\epsilon_3(2+w)]\}+(2-z)\{\alpha(x-2) \\ &\quad -\beta y-\alpha(x-2)[(x-2)^2+y^2/R^2]\}, \\ y' &= -(z+2)(y-b)+(2-z)\{\beta(x-2)-\alpha y \\ &\quad -\alpha y[(x-2)^2+y^2/R^2]\}, \\ \epsilon_1 z' &= (4-z^2)[z+2-m(x+2)]-\epsilon_1 cz, \\ \epsilon_2 w' &= (4-z^2)[z+2-m(x+2)]-\epsilon_2 cz \end{aligned} \tag{4}$$

with parameter values given in the caption of Fig. 3. The flow generated by this set of equations is such that (a) any three-dimensional projection of it presents self-intersections, and (b) the flow can be locally approximated by two-dimensional patches ($d=2$). The geometric prescription to create this flow is to induce an oscillation in the coordinates of the point that attracts the trajectories in the upper branch of the fast manifold ($z \approx 2$). Therefore, one expects a flow that is not completely unrelated to the previous one: the disk for $z \approx -2$ and the existence of a small branch from this central disk into itself should be preserved. On the other hand, it is reasonable to expect a higher degree of complexity, as a new dynamic ingredient was added.

Table II contains the vertices of the 11 cells displayed in Fig. 3(b) (with the vertices arbitrarily labeled from 1 to 24). It is worth remarking that, even if Fig. 3 displays a three-dimensional projection of the strange attractor, the construction of the complex of cells and the calculation of the homology groups are entirely performed in four dimensions (x,y,z,w); in other words, results are completely independent of the projection, chosen with the sole aim of illustrating our example. From the information in this table, one can compute the homology groups describing the complex (through calculations such as the one explained in detail in the Appendix). This gives rise to

$$H_0 \approx \mathcal{Z}, H_1 \approx \mathcal{Z}^4, H_2 \approx 0,$$

which indicates that there is one connected component, no cavities, and four loops. In terms of the vertices written in the table, these four closed paths are as follows: the first loop $L_1 = \langle 7,9\rangle - \langle 7,13\rangle + \langle 9,15\rangle - \langle 13,14\rangle - \langle 14,16\rangle + \langle 15,16\rangle$, the second loop $L_2 = -\langle 7,9\rangle + \langle 7,13\rangle - \langle 9,10\rangle - \langle 10,22\rangle + \langle 13,14\rangle + \langle 14,22\rangle$, the third loop $L_3 = -\langle 3,4\rangle + \langle 3,7\rangle - \langle 4,5\rangle - \langle 5,23\rangle + \langle 7,9\rangle + \langle 9,10\rangle + \langle 10,23\rangle$, and the

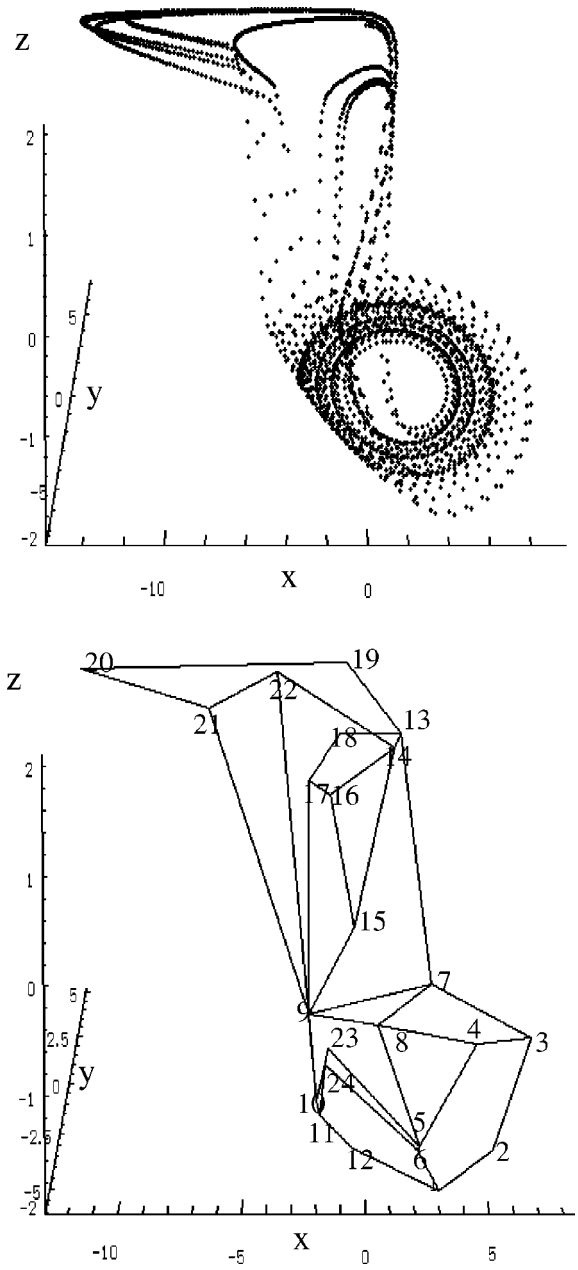

FIG. 3. The three-dimensional projection (x,y,z) of the strange attractor generated by the integration of the system of Eqs. (3), with the following set of parameters: $a=7$, $d=0.5$, $\alpha=0.3$, $\beta=7$, $\epsilon_1=0.165$, $\epsilon_2=0.01$, $\epsilon_3=2$ (a). Display of the 11 cells making up the complex obtained as explained in Sec. IV (b).

fourth loop $L_4=\langle 4,5\rangle-\langle 4,8\rangle+\langle 5,8\rangle$. One corresponds to the path around the hole of a central disk. The other three exist along the three branches of the complex, one of which reinjects flow from the outer region of the central disk to its inner part, and the other two stretch and fold the flow at the outer part of the central disk to reinject it. Notice that the geometry does not seem to be that different from what was obtained in the example of the preceding section. The main difference is that in the present case, one of the two branches that emerges from the central disk bifurcates in two strips, one of which twists before gluing.

TABLE II. Vertices of the oriented cells corresponding to the cell decomposition of the chaotic flow shown in Fig. 3.

Cell	Vertices
1	1,2,3,4,5,6
2	4,3,7,8
3	8,7,9
4	9,10,11,12,1,6,5,8
5	7,9,15,14,13
6	9,15,16,17
7	17,16,14,13,18
8	14,13,19,20,21,22
9	21,22,10,9
10	6,5,23,24
11	24,11,10,23

VII. CONCLUSIONS

The analysis of time-series data has been deeply enriched by the tools of nonlinear dynamics. Once that complexity is found to be compatible with simple deterministic rules, the analysis of complex time-series data has to address (a) whether the system is being ruled by a simple deterministic prescription; (b) if this is the case, whether it possible to model this rule; and finally (c), how to refute or validate a model. Along these lines, a topological approach toward time-series data consists in finding the branched manifolds that could hold all the periodic orbits found to coexist with given complex time-series data. This approach has two major shortcomings: (a) the dimensionality of the system under study was bound to be lower than or equal to 3 (since the compatibility between the flow and the branched manifold was determined through the knot properties of the periodic orbits in either case), and (b) the size of the data file had to be large enough to enable us the reconstruction of several periodic orbits [10,11].

In this work, we describe branched manifolds through homologies. This allows us to study situations in which the flows exist in manifolds of dimension larger than 3, as well as reasonably small time-series data (as the method does not rely on the characterization of periodic orbits). Our calculations begin by building complexes that summarize how to glue the cells that approximate the data. Codes that manipulate algebraically this information allow us to identify chain groups, boundary maps, cyclic groups, and homology groups. We can also explicitly build the generators of those groups and determine the orientability of the complex through the definition and calculation of the orientability chains.

In this work, we wrote the homological description of three branched manifolds, as well as the complexes approximating numerical flows (of three- and four-dimensional systems, respectively).

ACKNOWLEDGMENTS

This work has been partially funded by Fundación Antorchas, UBA (EX290), CEE (CI1 CT93-0331), and CONICET.

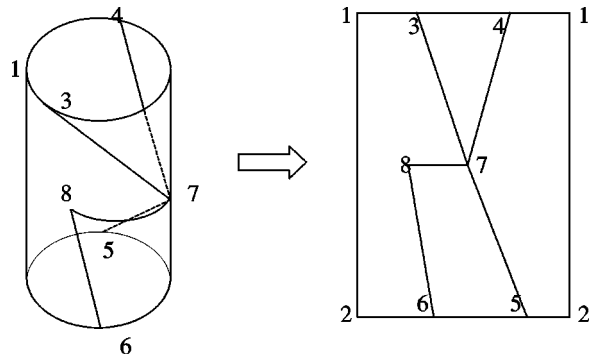

FIG. 4. Arbitrary cell decomposition of a cylinder with its nonsimplex complex. Vertices are numbered from 1 to 8.

Discussions with S. Ponce Dawson and I. Loisseau are acknowledged. We thank Bob Gilmore for enlightening comments.

APPENDIX

Let us list the basic steps to compute the homology groups through a simple example. Figure 4 shows an arbitrary cell decomposition of a cylinder, which gives rise to a nonsimplex complex in which the vertices have been labeled with numbers from 1 to 8. We follow the steps listed in Sec. II to calculate B_k, Z_k, and H_k for $k=1$.

(i) The list of vertices present in Fig. 4 is summarized in Table III. In order to represent algebraically the boundary maps of this complex, one needs two matrices: In the first matrix, every 0-cell or vertex is assigned a column. The rows correspond to the 1-cells. As the action of the operator ∂ on an oriented 1-cell yields the terminal vertex minus the initial vertex, the rows of this matrix are vectors with a 1 in the column corresponding to the terminal vertex and a -1 in the column of the initial point. In the case of our cylinder, this matrix reads

∂	1	2	3	4	5	6	7	8
$\langle 1,2\rangle$	-1	1	0	0	0	0	0	0
$\langle 1,3\rangle$	-1	0	1	0	0	0	0	0
$\langle 1,4\rangle$	-1	0	0	1	0	0	0	0
$\langle 2,5\rangle$	0	-1	0	0	1	0	0	0
$\langle 2,6\rangle$	0	-1	0	0	0	1	0	0
$\langle 3,4\rangle$	0	0	-1	1	0	0	0	0
$\langle 3,7\rangle$	0	0	1	0	0	0	1	0
$\langle 4,7\rangle$	0	0	0	-1	0	0	1	0
$\langle 5,6\rangle$	0	0	0	0	-1	1	0	0
$\langle 5,7\rangle$	0	0	0	0	-1	0	1	0
$\langle 6,8\rangle$	0	0	0	0	0	-1	0	1
$\langle 7,8\rangle$	0	0	0	0	0	0	-1	1

In the second matrix, every 1-cell is assigned a column as the rows correspond to the 2-cells. The border of a 2-cell is a chain of 1-cells with sign $+$ if the direction of the 1-cell is consistent with the clockwise or anticlockwise orientation of the vertices of the 2-cell. In our example, the transpose of the second matrix (M^t) is equal to

∂^t	$\langle 1,3,7,8,6,2\rangle$	$\langle 3,7,4\rangle$	$\langle 4,7,5,2,1\rangle$	$\langle 6,8,7,5\rangle$
$\langle 1,2\rangle$	-1	0	-1	0
$\langle 1,3\rangle$	1	0	0	0
$\langle 1,4\rangle$	0	0	1	0
$\langle 2,5\rangle$	0	0	-1	0
$\langle 2,6\rangle$	-1	0	0	0
$\langle 3,4\rangle$	0	-1	0	0
$\langle 3,7\rangle$	1	1	0	0
$\langle 4,7\rangle$	0	-1	1	0
$\langle 5,6\rangle$	0	0	0	1
$\langle 5,7\rangle$	0	0	-1	-1
$\langle 6,8\rangle$	-1	0	0	1
$\langle 7,8\rangle$	1	0	0	-1

(ii) To calculate B_1, one just needs the linearly independent rows of the matrix M. In the example of the cylinder, the rows of M are linearly independent, and thus B_1 consists of the four 1-chains listed as columns above.

(iii) The 1-cycles are the null space of the transpose of the first matrix. In our example, this calculation renders five 1-cycles in the complex. We illustrate Z_1 as follows: $Z_1=[[-\langle 1,2\rangle+\langle 1,3\rangle-\langle 2,6\rangle+\langle 3,7\rangle-\langle 6,8\rangle+\langle 7,8\rangle, +\langle 1,2\rangle-\langle 1,3\rangle+\langle 2,5\rangle-\langle 3,7\rangle+\langle 5,7\rangle, +\langle 2,5\rangle-\langle 2,6\rangle+\langle 5,6\rangle, -\langle 1,3\rangle+\langle 1,4\rangle-\langle 3,7\rangle+\langle 4,7\rangle, +\langle 1,3\rangle-\langle 1,4\rangle+\langle 3,4\rangle]]$.

(iv) Expressing now the elements of B_1 as linear combinations of the elements of Z_1, one obtains chains of 1-cycles that by definition are homologous to zero. This establishes homology relations between the 1-cycles, which one must take into account to obtain H_1.

(v) With the relations obtained in step (iv), one can conclude that of the five 1-cycles, only one is homologically independent. In other words, the homology relations tell us that the first four 1-cycles are homologous to the last (any information carried by the first loops is also carried by the last). The final result is

$$H_1=[[+\langle 1,3\rangle-\langle 1,4\rangle+\langle 3,4\rangle]]$$

with a group structure $H_1\approx\mathcal{Z}$, which reveals that there is only one nontrivial loop in a cylinder. This conclusion is independent of the particular cell decomposition we have chosen, as it denotes a geometric property of the cylinder itself.

TABLE III. Vertices of the oriented cells corresponding to the cell decomposition of the cylinder shown in Fig. 4.

Cell	Vertices
1	1,3,7,8,6,2
2	3,7,4
3	4,7,5,2,1
4	6,8,7,5

[1] H. D. I. Abarbanel, R. Brown, J. J. Sidorowich, and L. Sh. Tsimring, Rev. Mod. Phys. **65**, 1331 (1993).
[2] G. B. Mindlin, H. G. Solari, R. Gilmore, X. J. Hou, and N. B. Tufillaro, Phys. Rev. Lett. **64**, 2350 (1990).
[3] G. B. Mindlin, H. G. Solari, M. A. Natiello, R. Gilmore, and X. Hou, J. Nonlinear Sci. **1**, 147 (1991).
[4] Denisse Sciamarella and G. B. Mindlin, Phys. Rev. Lett. **82**, 1450 (1999).
[5] M. R. Muldoon, R. S. MacKay, J. P Huke, and D. S. Broomhead, Physica D **65**, 1 (1993).
[6] L. C. Kinsey, *Topology of Surfaces*, UTM Series (Springer Verlag, New York, 1993).
[7] J. Birman and R. Williams, Topology **22**, 47 (1983).
[8] P. Holmes and R. Williams, Arch. Ration. Mech. Anal. **90**, 115 (1985).
[9] B. Deng, Int. J. Bifurcation Chaos Appl. Sci. Eng. **4**, 823 (1994).
[10] G. B. Mindlin and R. Gilmore, Physica D **58**, 229 (1992).
[11] R. Gilmore, Rev. Mod. Phys. **70**, 1455 (1998).